Balancing optimization of a multiple speeds flexible rotor

Jianfei Yao[a,b,c], Fengyu Yang[b,c],Yongfei Su[a,c], Fabrizio Scarpa[d,e], Jinji Gao[a,b,c]

[a] Beijing Key Laboratory of Health Monitoring and Self-recoverying for High-end Mechanical Equipment, Beijing University of Chemical Technology, Beijing, 100029, China

[b] Key Lab of Engine Health Monitoring-Control and Networking of Ministry of Education, Beijing University of Chemical Technology, Beijing, 100029, China

[c] College of Mechanical and Electrical Engineering, Beijing University of Chemical Technology, Beijing, 100029, China

[d] Bristol Composites Institute (ACCIS), University of Bristol, Bristol BS8 1TR, UK

[e] Dynamics and Control Research Group (DCRG), University of Bristol, Bristol BS8 1TR, UK

(Corresponding author: Jianfei Yao, Email: yaojf@mail.buct.edu.cn)

Abstract

The paper describes a method to perform the dynamic balancing of multiple speeds flexible rotors. The method is integrated with a dual-objective optimization method (DOM) to overcome the shortcomings that classical least squares influence coefficient method (LSM) may induce by generating excessive residual vibrations at specific rotor speeds when a flexible rotor is dynamically balanced. The technique here described involves two consecutive optimization steps. During the first step an optimal correction weight of the parameters population is identified by using a genetic algorithm（GA）applied to an objective function made from the sum of the squares of the residual vibrations. This first optimization step is performed multiple times to obtain a set of optimized correction weights. A second optimization process is then performed by minimizing the maximum value of the residual vibration of the rotor. Each correction weight belonging to the first optimization set is embedded into an equation that represents the residual vibration to obtain the final optimal correction weight. The validity of the proposed method is verified by simulations and experiments related to a double-disc rotor-bearing system. The results show the DOM provides a more effective balancing strategy than the one obtained from using GA and classical LSM.

Keywords: Flexible rotor; Rotor balancing; Dual-objective optimization; Genetic algorithm; Least squares method.

1 Introduction

Rotor balancing is a key technology to ensure smooth, safe and reliable operations for rotating machinery. Rotor unbalance occurs when the center line of the rotor mass does not coincide with the axis of rotation. The rotor unbalance may result from imperfections occurring during the manufacturing process or as a result of various operating factors (loss of integrity of the machine, thermal effects and buildup of unbalance on the shaft and on the surfaces of the rotor). Rotor unbalance may lead to malfunction, such as rotor rub-impact [1] and bearing wear [2], and even to catastrophic failure. Rotor dynamic balancing is therefore necessary to guarantee a robust and reliable operation for rotating machines.

The current methods used to determine the balancing of flexible rotors mainly consist in modal balancing [3] and the influence coefficient method（ICM）[4]. Holo-balancing [5-7], active balancing [8] and the balancing method without trial weights [9-13] have all been recently proposed to complement the traditional dynamic balancing methods used in industry. The modal balancing method can be effectively used to account for any unbalance of the rotor when the full modal set of the system is known. By balancing the various modes of the rotor, the unbalanced components are eliminated and the entire rotor system is balanced. Han [14] has proposed a new generalized mode balancing for non-isotropic rotor systems, based on the derived unbalance modal responses from the complete modal analysis of a non-isotropic rotor systems. Deepthikumar et al. [15] have experimentally validated the performance of distributed unbalance by using modal balancing in flexible rotors having both unbalance and bow. Khulief et al. [16]

have proposed a modally tuned influence coefficients method for the low-speed balancing of flexible rotors. The method combines the advantages of the influence coefficient method and modal balancing to achieve the low-speed dynamic balancing of a high-speed rotor. The modal shape of the rotor must be however estimated empirically to use this method efficiently. Tresser et al. [17] have proposed a novel balancing technique for super-critical rotating structures using parameter excitation and modal identification at low-speed. Li et al. [18] have combined the modal balancing method with finite elements to propose a modal balancing technique without trial weights. In this case the dynamic characteristics of the rotor are obtained by using a finite element model, while the correction weights are calculated using the transient and the steady-state responses of the rotor at the balancing speed.

The ICM approach is simple, easy to operate and widely used for on-site dynamic balancing. The ICM works by designing the balancing of the rotor based on linear relationships between the corrected weights and the measured rotational vibrations. Wang [19] has suggested a strategy to balance a flexible rotor by sequential quadratic programming (SQP) using the ICM and the holospectrum techniques. Messager et al. [20] have proposed a discrete optimization method to balance a rotor in two planes by considering real constraints related to the available standard masses and predefined angular positions. This approach minimizes the residual unbalancing effects, but it can be only applied to rigid rotors with rigid supports. Saldarriaga et al. [21] have presented a flexible rotors dynamic balancing method based on an inverse problem approach. The method uses the unbalance masses and their corresponding angular positions as the design variables in a pseudo-random optimization, and obtains the correction weights based on the parameters of the rotor system model. In practice, this method does not present the drawbacks provided by the traditional dynamic balancing method, however it needs an accurate set of parameters to define the rotor model. Kang et al. [22] have introduced a technique that consists in minimizing the number of conditions in the Hermitian matrix of the influence coefficients by selecting the sensor locations and the balancing planes. This approach allows to improve the accuracy and the efficiency of the rotor balancing. Although this method can help optimize the balancing process, reducing residual vibrations and correcting weights by minimizing the number of conditions requires further study. Untaroiu et al. [23] have identified some suitable constraints on the level of the residual vibrations and the magnitude of the correction weights, and have converted those into a linear matrix inequality form, which has been solved by numerical convex optimization to obtain the correction weights. Li et al [24] have proposed a robust optimal balancing method for high-speed rotating machinery that formulates the high-speed flexible rotor balancing problem as a convex optimization problem. This method considers the use of influence coefficients, the vibration of the unbalance rotor and the correction weights as random parameters. Carvalho et al [25] have proposed a robust balancing approach based on fuzzy logic to reduce the sensitivity of the system to operational fluctuations. The method however can show robustness only when handling changes in the operating conditions of the rotor, fluctuations occurring during the vibration responses require to develop specific fuzzy sets for the rotor. In Refs. [26], the identification and balancing of the flexible rotor unbalance parameters were carried out by an optimization algorithm.

The dynamic balancing of a flexible rotor involves the knowledge of multiple measuring points, multi-speeds and multiple correction planes. For example, the use of the ICM in a flexible rotor at a specific speed leads to a rotor unbalance that creates centrifugal inertia and therefore modify the deformation of the rotor, and lead to further changes of the rotor mass distribution when the speed is altered. Goodman [4] has pioneered the use of the least squares method to identify influence coefficients for solving the problem. There are however limitations when using LSM in flexible rotors, because the residual vibrations of some measuring points are often quite large at a specific speed. To counteract this problem, the authors believe that, when performing multi-speeds balancing of flexible rotor, we should not only pay attention to the sum of the squares of the residual

vibrations, but also to the maximum value of the residual vibration. This paper therefore proposes a dynamic balancing method for flexible rotors that combines a dual-objective optimization procedure applied to multiple speeds of the rotor. The optimization is performed using an objective function calculated from the sum of the squares of the residual vibrations of the rotor. A genetic algorithm is here used to perform global searches of the objective function to obtain a set of optimized correction weights. A second optimization run is then performed by minimizing the maximum value of the residual vibration of the rotor. Each correction weight from a solution of the first optimization is brought into the equation that represents the residual vibration, to finally obtain an optimal correction weight. Simulations and experiments are carried out to verify the validity of the proposed method in a double-disc rotor-bearing system. The results show that the balancing and optimization procedure described in this work leads to an improved balance effect than the one offered by GA and the classical LSM.

2 Methodology

2.1 Least squares influence coefficient method

When the ICM is used for the dynamic balancing of a flexible rotor, it is necessary to select multiple speeds at the same time to balance the flexible rotor within a specific range of speeds. Within the ICM, one needs to consider K correction planes, M measurement points, and N rotation speeds. The equilibrium condition can be expressed as:

$$\boldsymbol{AU} + \boldsymbol{O} = \boldsymbol{R} \tag{1}$$

Where $\boldsymbol{A}$ is the matrix of the influence coefficients:

$$\boldsymbol{A}=\begin{bmatrix} \boldsymbol{\alpha}_{11} & \boldsymbol{\alpha}_{12} & \boldsymbol{\alpha}_{13} & \cdots & \boldsymbol{\alpha}_{1K} \\ \boldsymbol{\alpha}_{21} & \boldsymbol{\alpha}_{22} & \boldsymbol{\alpha}_{23} & \cdots & \boldsymbol{\alpha}_{2K} \\ \boldsymbol{\alpha}_{31} & \boldsymbol{\alpha}_{32} & \boldsymbol{\alpha}_{33} & \cdots & \boldsymbol{\alpha}_{3K} \\ \vdots & \vdots & \vdots & \ddots & \vdots \\ \boldsymbol{\alpha}_{(N\times M)1} & \boldsymbol{\alpha}_{(N\times M)2} & \boldsymbol{\alpha}_{(N\times M)3} & \cdots & \boldsymbol{\alpha}_{(N\times M)K} \end{bmatrix} \tag{2-a}$$

$\boldsymbol{U}$ is vector of the correction weights,

$$\boldsymbol{U}=\left(\boldsymbol{u}_1,\ \boldsymbol{u}_2,\ \cdots,\ \boldsymbol{u}_i,\ \cdots,\ \boldsymbol{u}_K\right)^{\mathrm{T}},(i=1,2,3,\cdots,K) \tag{2-b}$$

$\boldsymbol{O}$ is the original vibration (OV),

$$\boldsymbol{O}=\left(\boldsymbol{o}_1,\ \boldsymbol{o}_2,\ \cdots,\ \boldsymbol{o}_i,\ \cdots,\ \boldsymbol{o}_{(N\times M)}\right)^{\mathrm{T}},(i=1,2,3,\cdots,N\times M) \tag{2-c}$$

$\boldsymbol{R}$ is the error vector and is also called residual vibration,

$$\boldsymbol{R}=\left(\boldsymbol{r}_1,\ \boldsymbol{r}_2,\ \cdots,\ \boldsymbol{r}_i,\ \cdots,\ \boldsymbol{r}_{(N\times M)}\right)^{\mathrm{T}},(i=1,2,3,\cdots,N\times M) \tag{2-d}$$

The equation (1) can be expressed as

$$\begin{bmatrix} \boldsymbol{\alpha}_{11} & \boldsymbol{\alpha}_{12} & \boldsymbol{\alpha}_{13} & \cdots & \boldsymbol{\alpha}_{1K} \\ \boldsymbol{\alpha}_{21} & \boldsymbol{\alpha}_{22} & \boldsymbol{\alpha}_{23} & \cdots & \boldsymbol{\alpha}_{2K} \\ \boldsymbol{\alpha}_{31} & \boldsymbol{\alpha}_{32} & \boldsymbol{\alpha}_{33} & \cdots & \boldsymbol{\alpha}_{3K} \\ \vdots & \vdots & \vdots & \ddots & \vdots \\ \boldsymbol{\alpha}_{(N\times M)\times 1} & \boldsymbol{\alpha}_{(N\times M)\times 2} & \boldsymbol{\alpha}_{(N\times M)\times 3} & \cdots & \boldsymbol{\alpha}_{(N\times M)\times K} \end{bmatrix}\begin{bmatrix} \boldsymbol{u}_1 \\ \boldsymbol{u}_2 \\ \boldsymbol{u}_3 \\ \vdots \\ \boldsymbol{u}_K \end{bmatrix}+\begin{bmatrix} \boldsymbol{o}_1 \\ \boldsymbol{o}_2 \\ \boldsymbol{o}_3 \\ \vdots \\ \boldsymbol{o}_{(N\times M)} \end{bmatrix}=\begin{bmatrix} \boldsymbol{r}_1 \\ \boldsymbol{r}_2 \\ \boldsymbol{r}_3 \\ \vdots \\ \boldsymbol{r}_{(N\times M)} \end{bmatrix} \tag{3}$$

Equation (3) contains $N\times M$ equations. When $N\times M=K$, the number of equations is equal to the number of the correction planes:

$$\boldsymbol{R} = \boldsymbol{0} \tag{4}$$

The equilibrium equation (3) has a unique solution:

$$\boldsymbol{U} = -\boldsymbol{A}^{-1}\boldsymbol{O} \tag{5}$$

When $N\times M<K$, the number of equations is lower than the number of the correction planes. This situation rarely

occurs during balancing. In practice, the number of the correction planes is limited, and often $N\times M>K$ i.e., the number of equations is greater than the number of the correction planes:

$$\boldsymbol{R} \neq \boldsymbol{0} \tag{6}$$

At this time, equation (3) is overdetermined and cannot be solved directly. Goodman adopts the least squares method to minimize the sum of square of residual vibration at each measurement point. Let f be the sum of square of residual vibration of each measuring location:

$$f = \min \sum_{i=1}^{N\times M} |\boldsymbol{r}_i|^2 \tag{7}$$

The minimum value condition can be used to solve the correction weight at each correction plane:

$$\boldsymbol{U} = -(\boldsymbol{A}^{*\mathrm{T}}\boldsymbol{A})^{-1}\boldsymbol{A}^{*\mathrm{T}}\boldsymbol{O} \tag{8}$$

The symbol "*" indicates a conjugate complex number.

The LSM solves a set of overdetermined equilibrium equations that represent the influence coefficients extracted from multiple points and planes, and at multiple speeds. The objective of the LSM in terms of balancing is the minimization of the sum of the squares of the residual vibrations of the measurement points at a specific target speed, and the resulting correction weights vector is called the optimal solution. The term optimal does not however indicate that the vibration of the rotor reaches a satisfactory level. A mere reach of the minimum of the sum of the squares of the residual vibrations in all the measurement points results - in some cases - in the identification of correction weights that may exceed the allowable value of the correction plane. Moreover, there is still a large residual vibration at some measuring points at specific rotor speeds when the solution is back-substituted into the equilibrium condition [27]. The optimal value provided by the LSM does not therefore necessarily correspond to a required physical solution, and a higher fidelity solution needs to be identified.

2.2 Dual-objective optimization of the balancing of a flexible rotor with multi-speeds

The minimization of the maximum of the residual vibration when the sum of the squared residual vibrations and the correction weights are constrained represents a case of multi-objective optimization. In multi-objective programming problems, different weights can usually be adopted according to the importance of each target. The multi-objective programming can be transformed into a single-objective problem by using a linear weighted summation [28]. However, due to their different size and dimensions some objective functions may tend to provide a more significant contribution to the global objective function than the others. The result is an overall objective function that it is not effectively optimized. A dual-objective optimization approach is therefore proposed to overcome the shortcomings of the LSM mentioned above.

2.2.1 The first optimization

The genetic algorithm is a random search method proposed by J.H. Holland [29] to simulate the natural selection and natural genetic mechanism during biological evolution. This technique has the ability to perform simultaneous multi-points searches and a global optimization in the solution space [30, 31]. Therefore, genetic algorithms have been extensively applied in mechanical design and optimization [32, 33]. Using equation (7) as the objective function of the first optimization, the optimization model is constructed as:

$$\begin{aligned} &\min\left(f = \sum_{i=1}^{N\times M} |\boldsymbol{r}_i|^2 \right); \\ &s.t\begin{cases} 0 \le \mathrm{mod}(\boldsymbol{u}_i) \le ub, \\ 0 \le \arg(\boldsymbol{u}_i) \le 2\pi, \\ i = 1,2,3,\cdots, \quad K. \end{cases} \end{aligned} \tag{9}$$

The reach of the minimum of the sum of the squares of the residual vibrations is required to perform the dynamic balancing of the flexible rotor. The individual with the smallest sum of the squares of the residual vibrations is the superior gene (the opposite is the inferior one). For the first optimization the $f_{\max}$ value is defined

as the maximum of the sum of the squared residual vibrations in the current population. The minimum of that sum is defined as $f_{\min}$. The maximum fitness function value can be expressed as:

$$Fit(f)_{\max} = f_{\max} - f_{\min} \tag{10}$$

If $Fit(f)_{\max}<\varepsilon$ (ε is the convergence condition) is satisfied, the corresponding correction weight is an output, otherwise the genetic operation is performed. The genetic algorithm optimizes Eq. (9) with the resulting final vector:

$$\boldsymbol{U}_i = \begin{cases} \boldsymbol{u}_1 \\ \boldsymbol{u}_2 \\ \vdots \\ \boldsymbol{u}_K \end{cases}$$

$\boldsymbol{u}_1$ represents the mass and phase of the correction plane 1. A solution of the correction weights C is obtained by solving the first optimization loop m times based on the genetic algorithm proposed above:

$$C = \{\boldsymbol{U}_1, \boldsymbol{U}_2, \boldsymbol{U}_i, \cdots, \boldsymbol{U}_m\} \tag{11}$$

2.2.2 The second optimization

The purpose of the second optimization procedure is to minimize the maximum of the residual vibration at each measurement point. A set of solutions C is here found that minimizes the infinite norm of the $\boldsymbol{R}$ vector.

Each set of weights is initially brought into equation (3). The residual vibration column vector $\boldsymbol{R}_k$ corresponding to the weight $\boldsymbol{U}_k$ is therefore corrected. The amplitude of the residual vibration of the i^{th} measuring point at the j^{th} rotational speed $\boldsymbol{r}_{ij}$ ($\boldsymbol{r}_{ij}=a_{ij}+ib_{ij}$, where a_{ij} is the real part and b_{ij} is the imaginary component) is:

$$\left|\boldsymbol{r}_{ij}\right| = \sqrt{a_{ij}^{\ 2} + b_{ij}^{\ 2}} \tag{12}$$

The maximum value of the residual vibration can be obtained from the elements of the residual vibration column vector. This step is repeated m times. A set of the maximum values of the residual vibration is therefore obtained:

$$\left\{\left|\boldsymbol{r}\right|\right\}_{\max} = \left\{\left|\boldsymbol{r}_{ij}\right|_{1.\max}, \quad \left|\boldsymbol{r}_{ij}\right|_{2.\max}, \quad \cdots, \quad \left|\boldsymbol{r}_{ij}\right|_{k.\max}\right\}, (k = 1,2,3,\cdots,m) \tag{13}$$

The minimum value of (13) is then found. The correction weight corresponding to the minimum value is the optimal correction weight vector.

The second optimization model is established as:

$$\begin{aligned} &\Delta = \min\left\|\boldsymbol{R}\right\|_{\infty} = \min\left(\max(\left|\boldsymbol{r}_{11}\right|, \left|\boldsymbol{r}_{12}\right|, \cdots, \left|\boldsymbol{r}_{ij}\right|, \cdots, \left|\boldsymbol{r}_{NM}\right|)\right); \\ &s.t \begin{cases} \boldsymbol{A}\boldsymbol{U}_k + \boldsymbol{O} = \boldsymbol{R}_k, \\ \boldsymbol{U}_k \in C, \\ k = 1,2,3,\cdots,m. \end{cases} \end{aligned} \tag{14}$$

The optimal correction weight can be obtained after the dual-objective optimization. The change of the initial population in each optimization run however results in modifications of the correction weights obtained from the first optimization. Therefore, the scheme of the final correction weight is obtained by calculating the average of the optimal correction weights obtained by performing multiple times.

The flow chart of the DOM proposed in this work is shown in Fig.1.

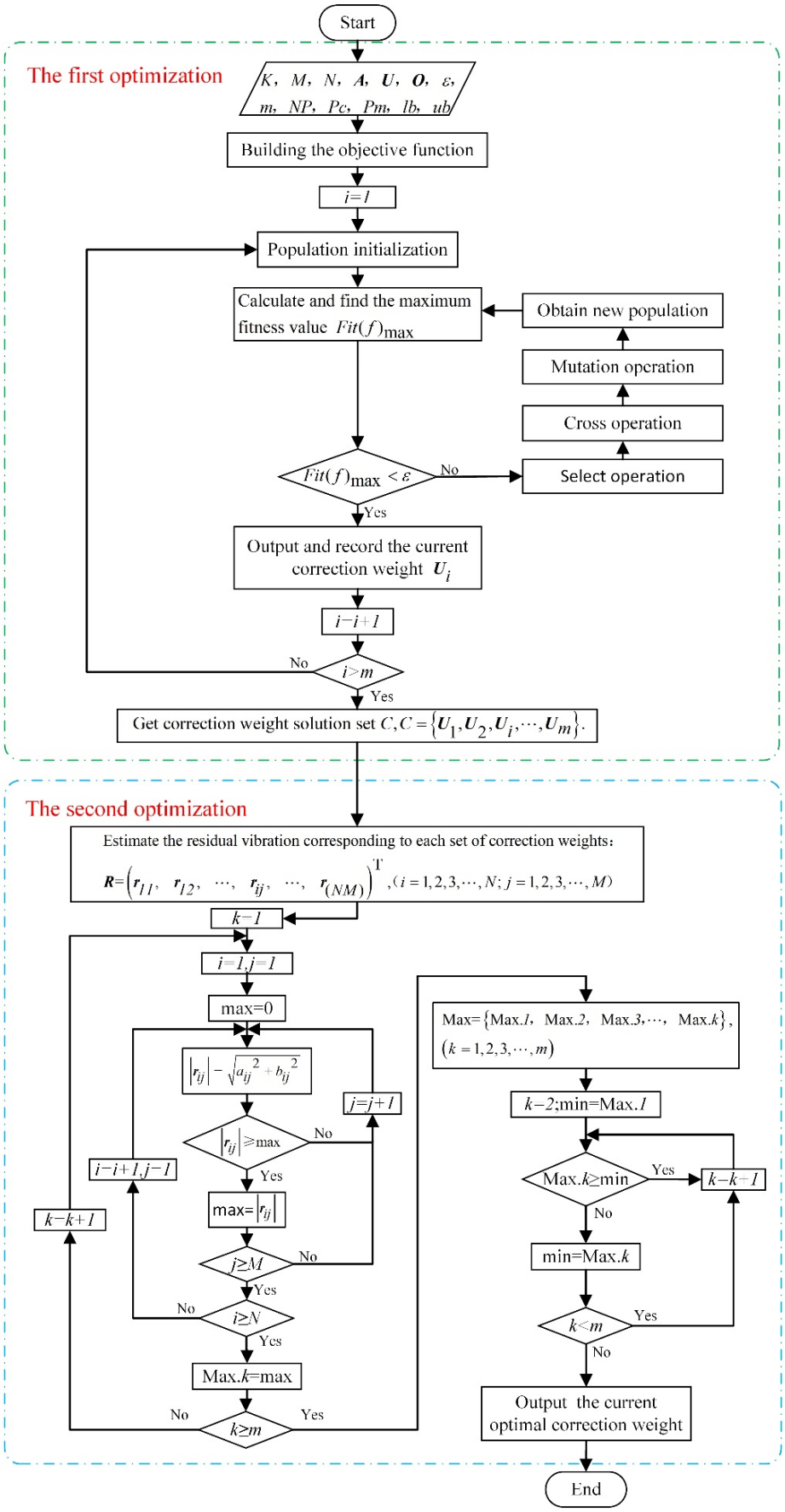

Fig.1 Flow chart of the DOM for flexible rotor balancing considering multi-speeds

3 Experimental and numerical test rig

3.1 Experimental test rig

The test rig representing a double-disc rotor-bearing system is shown in Fig.2. The rig is driven by a DC motor with a maximum speed of 12,000 rpm. A bellows coupling is used to connect the motor to the shaft. The test rig is mainly composed of a rotating shaft, two discs and two plain cylindrical bearings. The photoelectric sensor fixed on bearing#1 measures the rotor speed by receiving the reflected pulse. The displacements of the rotor are measured by using two eddy current displacement proximity probes. The specific parameters of the rig are shown in Table 1.

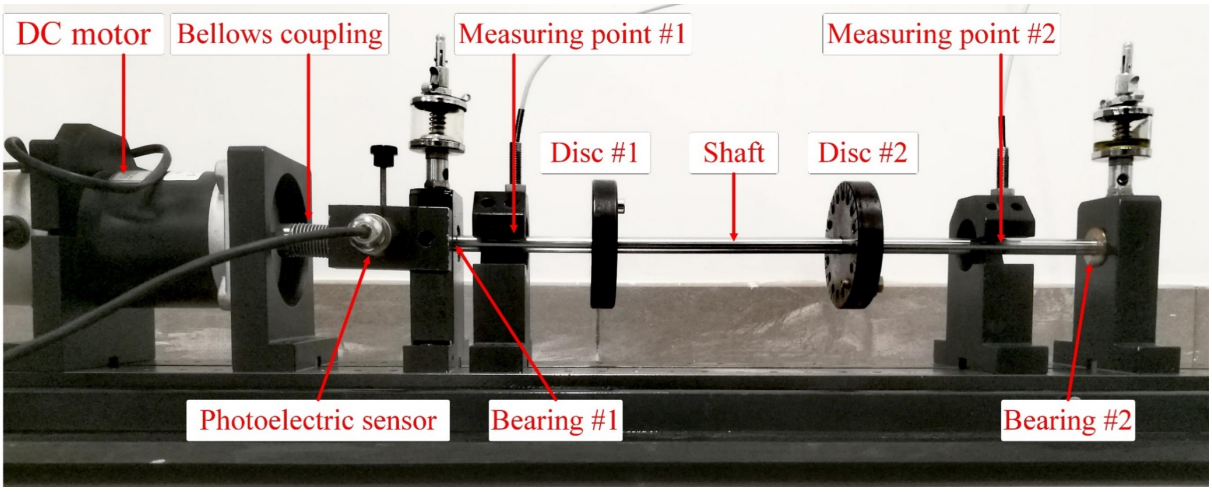

Fig.2 Test rig of double-disc rotor-bearing system

Table 1. Parameters of the test rig

Shaft parameters	
Material	Gcr15
Diameter	0.01m
Length	0.5m
Density	7810 kg/m^3
Modulus of elasticity	2.08×10^{11} N/m^2
Poisson ratio	0.3
Disc parameters	
Internal diameter	0.01m
External diameter	0.078m
Thickness	0.015m
Material	45steel
Mass	0.494kg
Bearing parameters	
Bearing journal diameter	0.01m
Clearance	1×10^{-5}m
Width	0.025m
Bearing span	0.42m
Lubricating oil parameters	
Density	0.88g/CC
Viscosity	32.5 cP

3.2 Modeling of the test rig

A finite element method is used to simulate the dynamics of the test (Fig.3). The numerical model mainly includes

three parts: the shaft, the discs and the bearings. According to the Timoshenko beam theory, the rotor shaft is discretized into finite beam elements with a total of 17 nodes and 16 units. Each node has two translational and two rotational degrees of freedom along the horizontal (x) and vertical (y) directions. The discs are added to the 6^{th} and 11^{th} nodes of the finite element model as lumped masses with polar and diameter moments of inertia. The bearings are modeled as concentrated translational springs and a viscous damper, and they are located at the 3^{rd} and 16^{th} nodes of the finite element model.

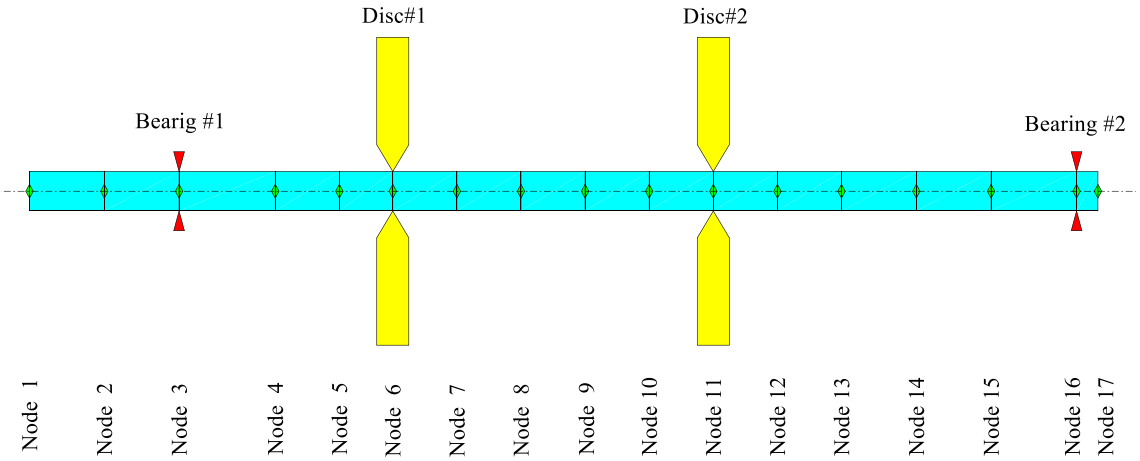

Fig.3 Finite element model of double-disc rotor-bearing system

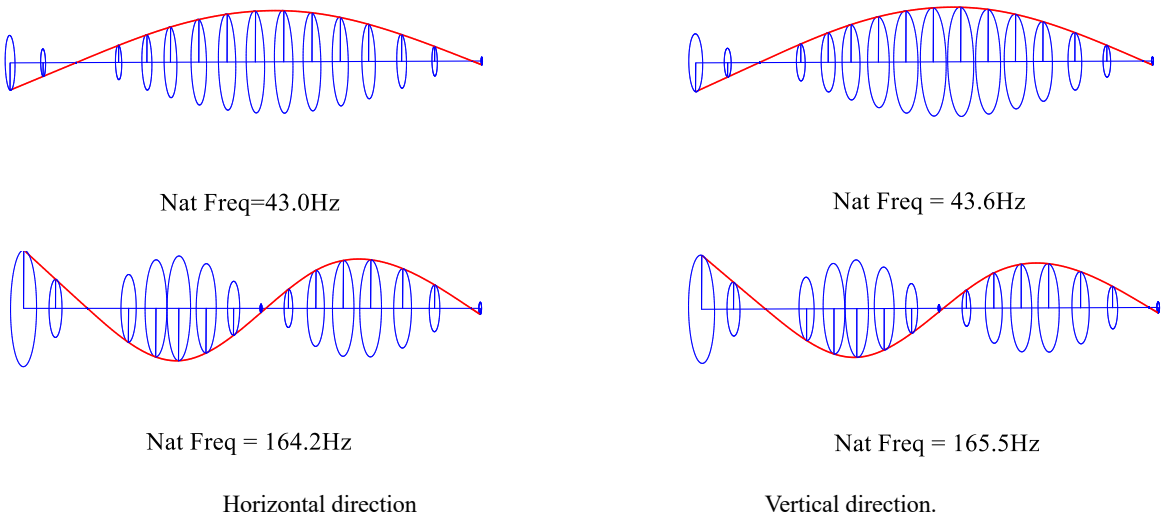

Fig.4 Modal mode diagram of the double-disc rotor-bearing system

The direction of the first measuring point of the test rig corresponds to the y direction of the 4^{th} node in the model. In a similar way, the second measuring point corresponds to the y direction of the 14^{th} node. The first two-order critical speeds and mode shapes of the double-disc rotor-bearing system are then calculated. Along the vertical direction, the first natural frequency is 43.6Hz and the corresponding critical speed is 2616rpm. The first critical speed of the measured test rig is 2650rpm, and that implies a 1.2% error against the numerical results. The finite element model of the double-disc rotor-bearing system developed here can therefore be considered sufficiently accurate to be used as a parametric and optimization platform.

4 Numerical simulations

Three balancing methods are presented in Table 2 for numerical simulation and experimental research.

Table 2. Balancing methods

Method	Equation/objective function	To solve the way
LSM	Equation (7)	direct solution
GA	Equation (9)	optimization solution
DOM	Equations (9) and (14)	optimization solution

In this paragraph the balancing effects of GA, LSM and DOM are compared and analyzed through two different cases. We assume force unbalance of the rotor bearing system in Case I, while in Case II we consider both force and the couple unbalance. The numerical simulation is based on the finite element model of the rotor developed in Section 3.2. The balancing target speeds are 1500 rpm, 4000 rpm and 6000 rpm, respectively.

Case I

We concentrate the force unbalance on the discs #1 and #2 of the finite element model. Discs #1 and #2 are also contained in the correction plane. The simulation process is as follows:

(1) An unbalance mass of 0.98g is added at $\angle 0^\circ$ to disc#1, and an unbalance mass of 1.31g is added at $\angle 180^\circ$ to disc#2. The vibration displacements of the 4^{th} and the 14^{th} nodes of the Finite Element along the y direction at each target speed are then calculated.

(2) A trial weight of 1.31g is added at $\angle 90^\circ$ to disc#1, and the displacements of the 4^{th} node and the 14^{th} node in the y direction at the target speeds (1500 rpm, 4000 rpm, and 6000 rpm) are computed. A trial weight of 1.31g is then added at $\angle 45^\circ$ on disc#2 after removing the previous trial weight. The displacements of the 4^{th} node and the 14^{th} node in the y direction at each target speed are then calculated. The corresponding influence coefficients are computed using the data from the original vibration response and the trial weight responses.

(3) The original vibration response and impact coefficient are substituted into the objective function, and the correction weight is calculated by GA and DOM respectively. Parameters are set in the calculation of the two balancing methods: the initial population size is set to 400, the crossover probability is 0.9, the mutation probability is 0.1, ε is 1×10^{-10}, the lower limit of the correction weight is 0, and the upper limit of the correction weight is 5g.

When the optimization algorithm is adopted, the results fluctuate to some extent. The two methods are therefore used to perform 50 simulations each, and the results are shown in Fig.5.

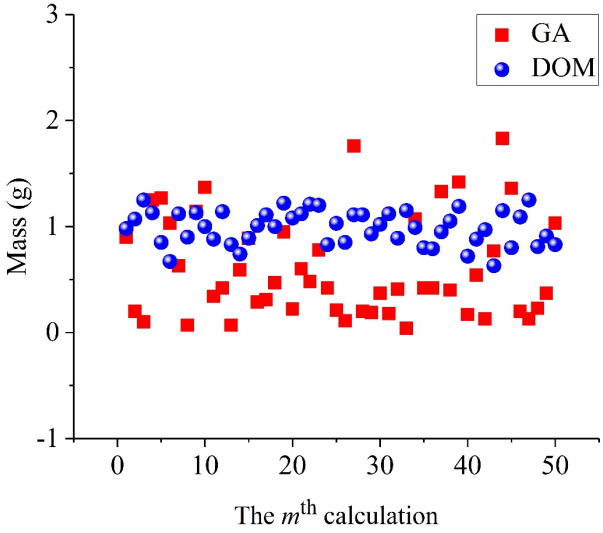

(a) Correction mass of disc #1

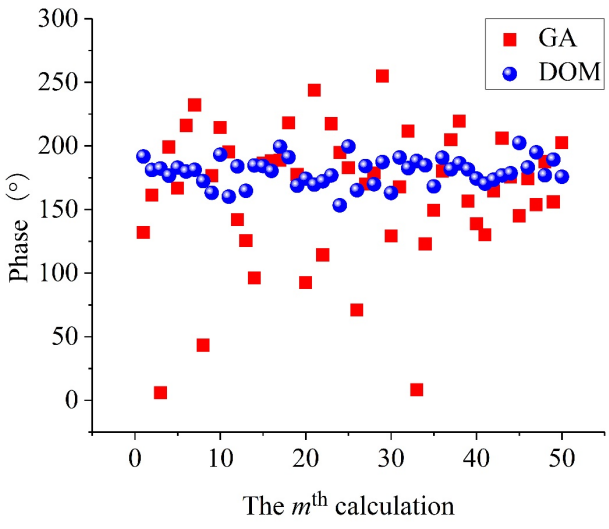

(b) Correction phase of disc #1

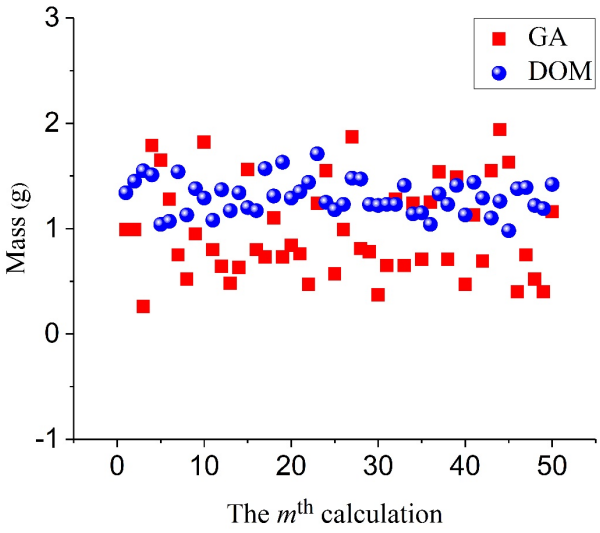

(c) Correction mass of disc #2

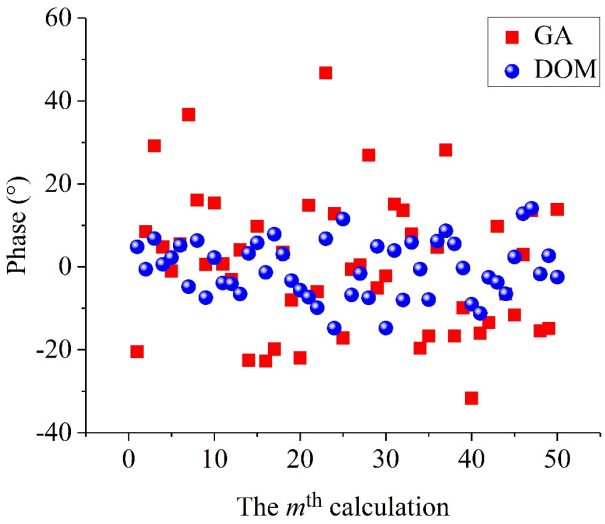

(d) Correction phase of disc #2

Fig.5 Correction weights calculation results

It is evident from Fig.5 that the results depend on the calculation times when the GA and DOM are used for the calculation of the balancing. The fluctuation range of the DOM results is however significantly smaller than the one provided by the GA.

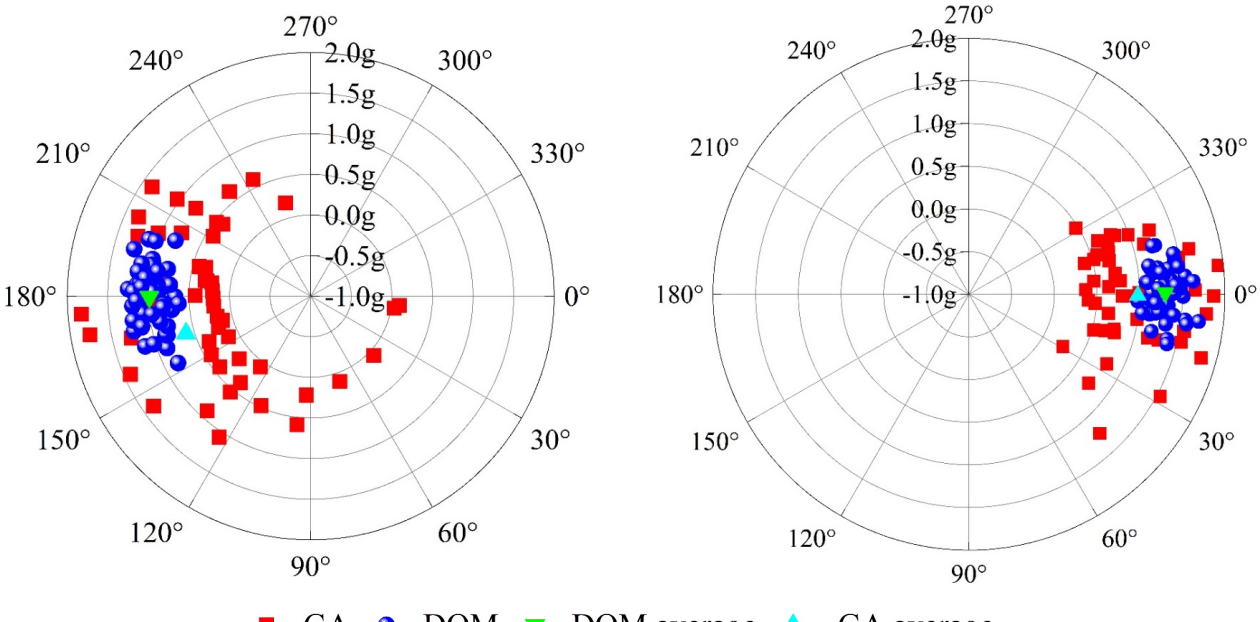

(a) Disc #1 (b) Disc #2

Fig.6 Correction weights

The correction mass and the phase of the same balancing plane in Fig.5 are represented in polar coordinates to obtain the correction weight (Fig.6). In that figure, the radial coordinate corresponds to the correction mass (positive is mass gain, negative is mass loss); the circumferential coordinate is the correction phase. This figure can more intuitively represent the fluctuation of the two methods. The average values here are calculated using the two methods and the final correction weights are shown in table 3.

Table 3. Correction weights

Method	Disc	Mass (g)	Error (%)	Phase (°)	Error (%)
	1	0.60	38.8	163.4	9.2

GA	2	0.98	25.2	0.5	0.1
DOM	1	0.99	1.02	179.7	0.2
	2	1.30	0.76	-0.4	0.1

We can therefore conclude that large fluctuations of the results are present every time the GA optimization of the balancing is performed, however the DOM results are relatively more stable. The correction weights are obtained by calculating the average of the results from the two methods. The results from the DOM calculations are quite accurate, while the GA ones have large errors that cannot be regarded as optimal weights. The DOM is therefore better than the GA in terms of stability and accuracy.

Case II

Force and couple unbalances are present in real rotor systems. On the basis of case I, both force and couple unbalances are both considered in case II. A couple unbalance of 3×10^{-5}N•m is added at 45° on disc#1. The resulting response as calculated following case I is shown in Fig.7 and Table 4.

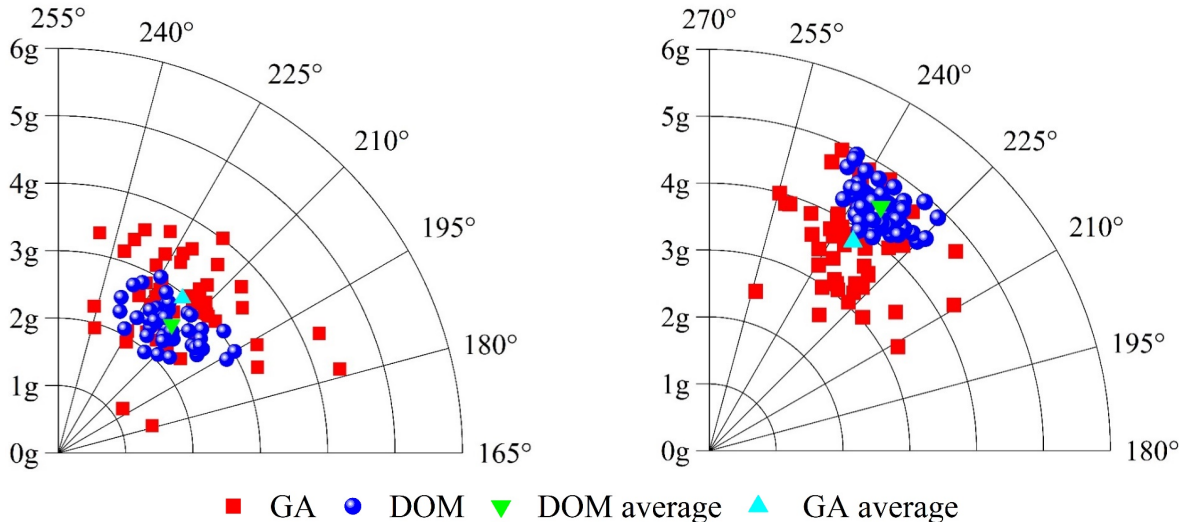

(a) Disc #1 (b) Disc #2

Fig.7 Correction weights

From the results of the case II, it is also evident that the fluctuations of the results derived by using the GA approach are still large compared to the DOM cases. The average value of all the calculated results for the two methods and the final balancing scheme are shown in Table 4. The calculation results of the LSM approach are also featured in Table 4.

Table 4. Correction weights

Method	Disc	Mass (g)	Phase (°)
GA	1	2.94	216.2
	2	3.79	235.5
LSM	1	2.46	211.7
	2	4.43	235.7
DOM	1	2.51	213.2
	2	4.39	235.6

The correction weights are also applied to the finite element model. The vibration responses of the speed-up process along the y direction of the 4th node and the 14th node are calculated (Fig.8). The residual vibration response and percentage of amplitude decrease at each target speed are shown in Fig.9.

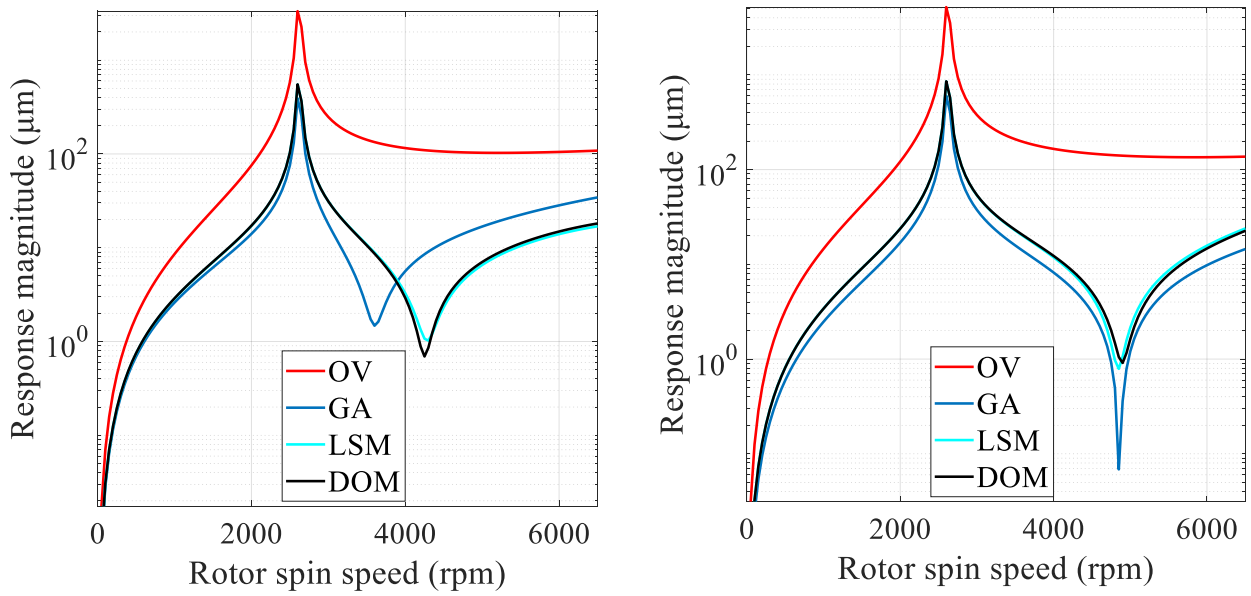

(a) The 4th node (b) The 14th node

Fig.8 Vibration response of the 4th and the 14th node along the y direction during speed-up before and after balancing

Compared to the original vibration values (Fig.8), all three methods can reduce the amplitude of the unbalance vibration response of the rotor. The balancing effect provided by the LSM and DOM approaches is almost the same, while the balance calculated through the GA is quite different from the former two methods. After the GA progressive balancing, the residual vibration of the 14th node is always lower than the one calculated using the first two methods. The residual vibration of the 4th node is slightly lower than the one of the first two methods at low speed, but significantly larger at high speed.

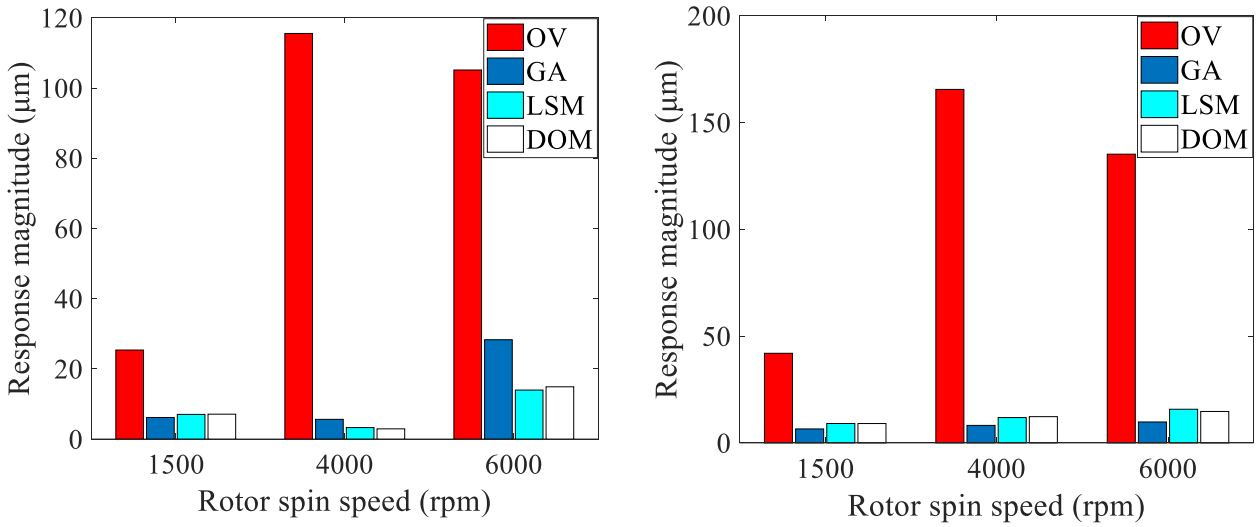

(a) The amplitude along the y direction of the 4th node at each target speed

(b) The amplitude along the y direction of the 14th node at each target speed

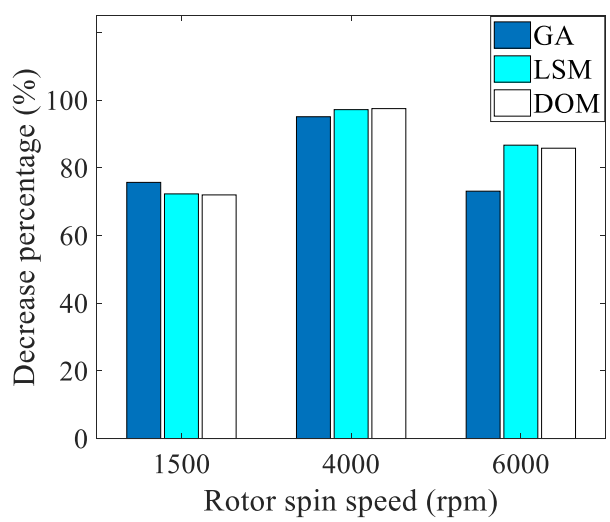

(c) The amplitude decrease along the y direction of the 4th node at each target speed

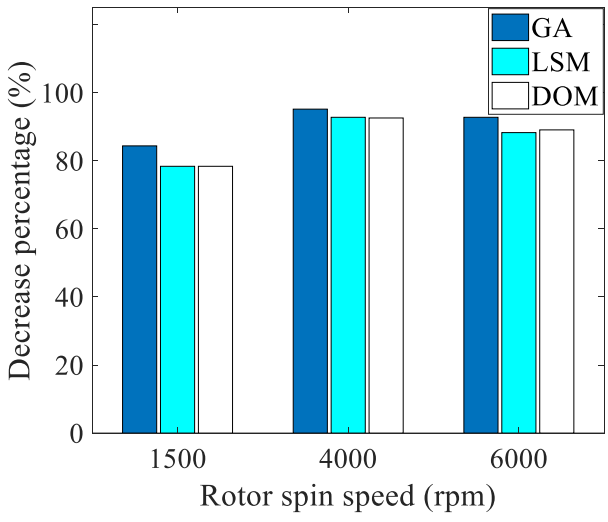

(d) The amplitude decrease along the y direction of the 14th node at each target speed

Fig.9 Vibration response and amplitude drop percentage at each target speed before and after balancing

After the three methods have been used to carry out the balancing, the maximum residual vibration value for each target speed appears at 6000rpm in the 4th node (Fig. 9). The maximum value of the residual vibration after balancing through LSM is 15.75μm, and 14.89μm when using DOM. The maximum value of residual vibration after GA balancing is 28.3μm. The maximum amplitude decreases after balancing using the LSM approach is 97.2%, while the minimum is 72.3%. After the DOM-based balancing the amplitude decreased by a maximum of 97.5% and a minimum of 72%. The GA balancing provided similar values (maximum and minimum decreases by 95.2% and 75.7% respectively). From simulations the sum of the squares of the original vibrations is 72465, while the sum of the squares of the residual vibrations is 726 when LSM is used for balancing (i.e., a 99% decrease).When DOM was used for balancing, the sum of the squares of the residual vibrations was 730; the GA-derived results provided a value of 1076, leading to a 98.5% decrease.

It is possible to observe an almost linear relationship between the unbalance and the unbalance vibration response in the finite element model. The three methods can all provide a good balancing effect. The DOM is better than the GA in terms of stability and accuracy in case I. In case II, the percentage decreases of the sum of the squares of the residual vibrations are very much equivalent, but the maximum value of the residual vibration obtained through GA is the largest, while the DOM method provides the minimum. From the above two simulation cases, one can conclude that the sum of the squares of the residual vibrations and the maximum value of residual vibration should be considered to engineer multi-speeds balancing of flexible rotor.

5 Experimental results

During the experiments the same parameters used for the simulations have been adopted. The target speeds are 1000 rpm, 1500 rpm, 4000 rpm, 5000 rpm and 6000 rpm. The experiment is carried out by adding the 1.31g trial weight at 90° on disc#1, and the trial weight response at each target speed is obtained. After removing the trial weight from disc#1, the same trial weight is added at 45° to disc#2, and the trial weight response at each target speed is then measured. The corresponding influence coefficients are calculated using the data of the original vibration response and the data from the vibration with the trial weight (Table 5).

Table 5. Original vibration, trial weight response

Speed (rpm)	Measuring point	Original vibration		disc#1 trial response		disc#2 trial response	
		Amp (μm)	Phase (°)	Amp (μm)	Phase (°)	Amp (μm)	Phase (°)

1000	1	33.67	72.08	31.42	67.08	31.74	73.36
	2	9.74	97.22	9.524	93.43	11.13	99.12
1500	1	41.94	55.76	34.88	57.16	36.44	70.41
	2	20.21	68.04	11.49	72.48	16.25	92.06
4000	1	46.95	-142.67	13.19	159.43	17.59	-79.69
	2	55.9	-141.74	36.59	-160.25	22.95	-81.63
5000	1	32.65	-150.1	10.42	96.91	9.67	-97.94
	2	39.85	-152.37	34.82	-169.9	12.1	-62.81
6000	1	27.32	-145.36	14.45	43.91	11.08	-118.29
	2	33.11	-163.73	41.03	-178.76	11.54	-15.12

Table 6. Influence coefficients at multi-speeds

Speed (rpm)	Measuring point	disc#1 influence coefficient		disc#2 influence coefficient	
		Amp (μm)	Phase (°)	Amp (μm)	Phase (°)
1000	1	2.76	-148.79	1.57	-173.01
	2	0.51	-103.40	1.09	67.15
1500	1	5.44	138.89	8.69	136.71
	2	6.72	152.24	6.50	152.10
4000	1	31.66	-37.04	32.05	-29.58
	2	18.45	-23.02	37.18	-30.85
5000	1	28.97	-45.46	21.21	-31.05
	2	9.48	-4.73	31.72	-34.30
6000	1	31.79	-52.15	13.87	-26.48
	2	9.52	47.75	33.11	-36.69

Experiments about the low speed and high-speed balancing at a single velocity are carried out using the ICM technique after obtaining the data from the original vibration of the rotor and the trial weight influence coefficient at the target speeds (Table 6). Experiments showing the dynamic balancing using the LSM and the DOM at multiple speeds have also been carried out.

Table 7. Two sets of single-speed balancing and correction weights considering the number of different speeds

Speed (rpm)	Theoretical weight				Actual weight	
	Method	Disc	Mass (g)	Phase (°)	Mass (g)	Phase (°)
1500	ICM	1	4.24	-72.4	3.77	-67.5
		2	7.45	102.8	7.23	112.5
5000	ICM	1	0.24	81.3	0.2	90
		2	1.21	59.3	1.23	67.5
1500 4000	LSM	1	0.15	-8.5	0.13	0
		2	1.58	75.4	1.58	67.5
	DOM	1	0.17	1.3	0.19	0
		2	1.69	78.6	1.68	67.5
1500 4000 6000	LSM	1	0.46	106	0.48	112.5
		2	1.24	59.3	1.23	67.5
	DOM	1	0.45	100.3	0.48	90
		2	1.36	67.7	1.36	67.5
1000、1500、4000、5000、6000	LSM	1	0.41	96	0.42	90
		2	1.21	59.9	1.23	67.5
		1	0.45	84.5	0.48	90

	DOM	2	1.28	67.3	1.31	67.5

After the calculation of the correction weights, the weighting schemes are selected and added to the threaded hole of the disc. The distance between the threaded hole and the axis is 0.03m and the distribution of the threaded hole on the disc is shown in Fig. 10.

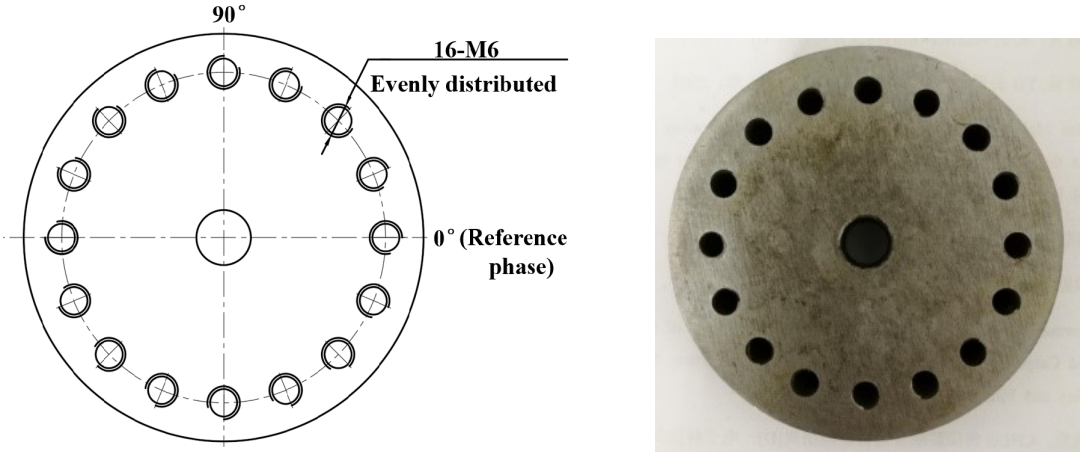

(a) (b)

Fig.10 Schematic diagram of the disc

5.1 Comparison of single-speed and multi-speeds balancing for the flexible rotor

In the experimental study, two sets of single-speed balancing related to the first critical speed are performed. One target speed for the balancing is 1500 rpm, the other is 5000 rpm. Experiments showing the dynamic balancing using the LSM and the DOM at 1500 rpm, 4000 rpm and 6000 rpm have also been carried out. The correction weights are shown in Table 7. The comparison of the results related to the optimization targets that consider the low and high single speeds and the multiple speeds balancing is shown in Fig.11-12.

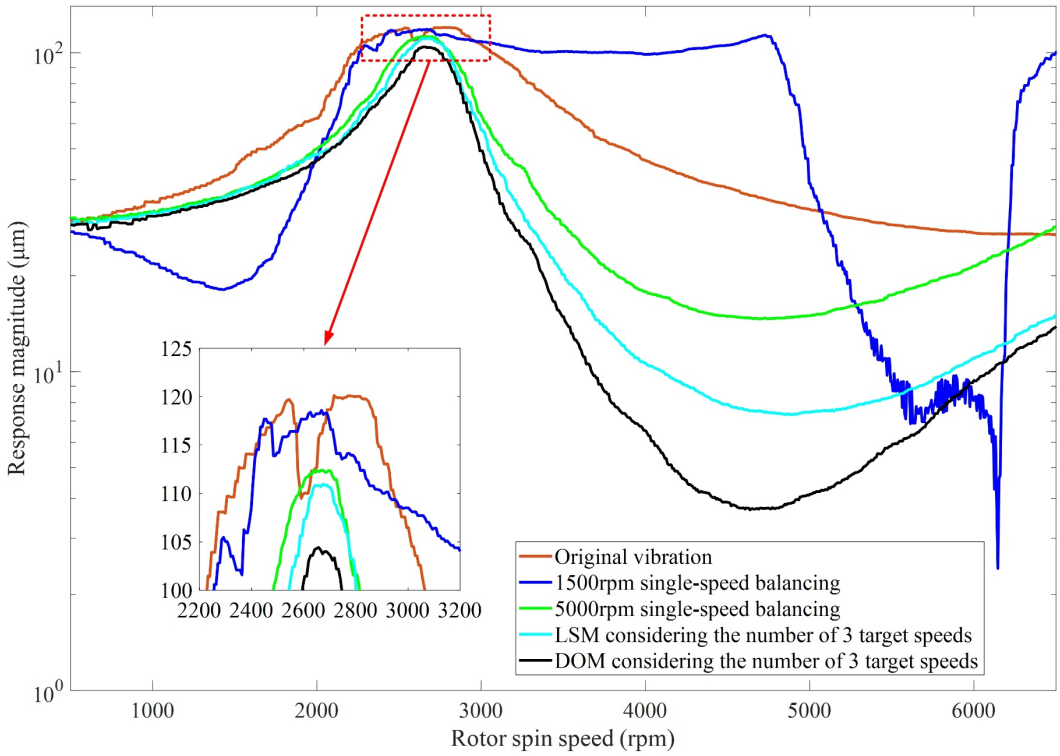

Fig.11 The speed-up curve when measuring point #1 before and after balancing

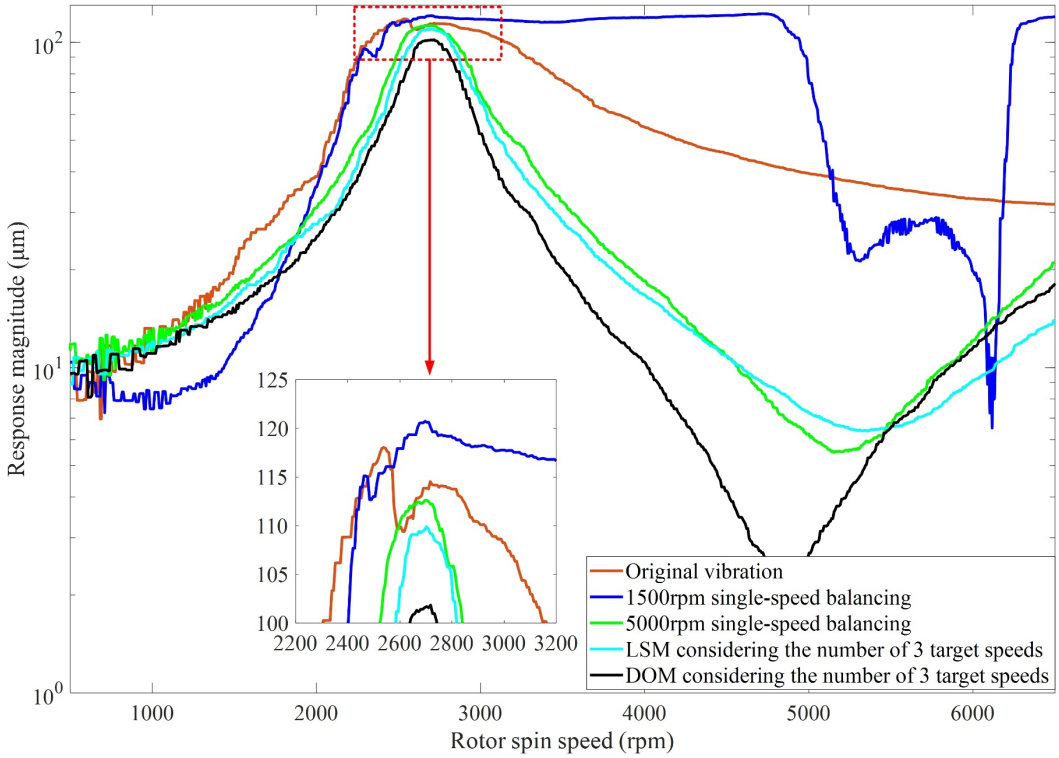

Fig.12 Speed-up curve when measuring point #2 before and after balancing

Table 8. Balancing effect of single-speed

Speed (rpm)	Measuring point	Original vibration (μm)	Amplitude after balancing (μm)	Percentage (%)
1500	1	42.96	18.59	56.7
	2	20.51	11.40	44.4
5000	1	32.26	14.97	53.6
	2	39.51	6.25	84.2

For a flexible rotor containing a first critical speed within the operational speed range, both single-speed and multiple speeds balancing provide a significant influence on the overall equilibrium effect of the system. When the balancing speed is lower than the first critical speed of the rotor and the number of balancing speeds is one, the vibration of the rotor at speeds below the first critical velocity drops significantly in the case of the low single-speed balancing (Figs. 11-12 and Table 8). The correction weight related to the low single-speed balancing however increases the rotor unbalance due to the flexible deformation of the rotor at higher velocities. The vibration amplitude of the rotor will be therefore larger for sizeable speed ranges, for which the velocity of the rotor is higher than the first critical speed. When the balancing speed is higher than the first critical velocity of the rotor, the vibration amplitude is reduced during speed-up and the balancing effect is more evident than the one produced by the low single-speed balancing. The LSM and DOM-led balancing here are performed using three balancing speeds. The balancing effect obtained by applying DOM is the most performing amongst the low single-speed balancing approaches, the high single-speed and the LSM balancing.

5.2 Sensitivity versus the number of target speeds

The correction weights identified by the two methods for the different numbers of speed were added to the test rig to perform separate balancing experiments. The speed-up curves of the measuring points 1 and 2 before and after balancing are shown in Figs.13 and 14. The vibration amplitudes of the respective target speeds are shown in Table 9.

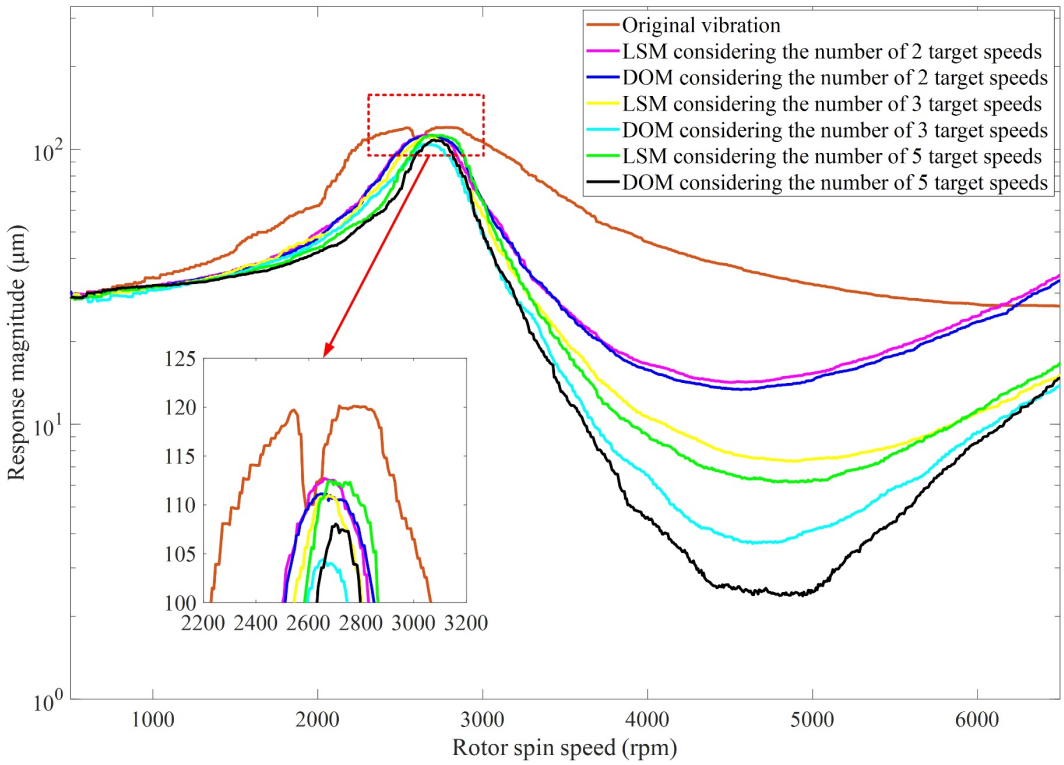

Fig.13 Speed-up curves at point #1 before and after balancing

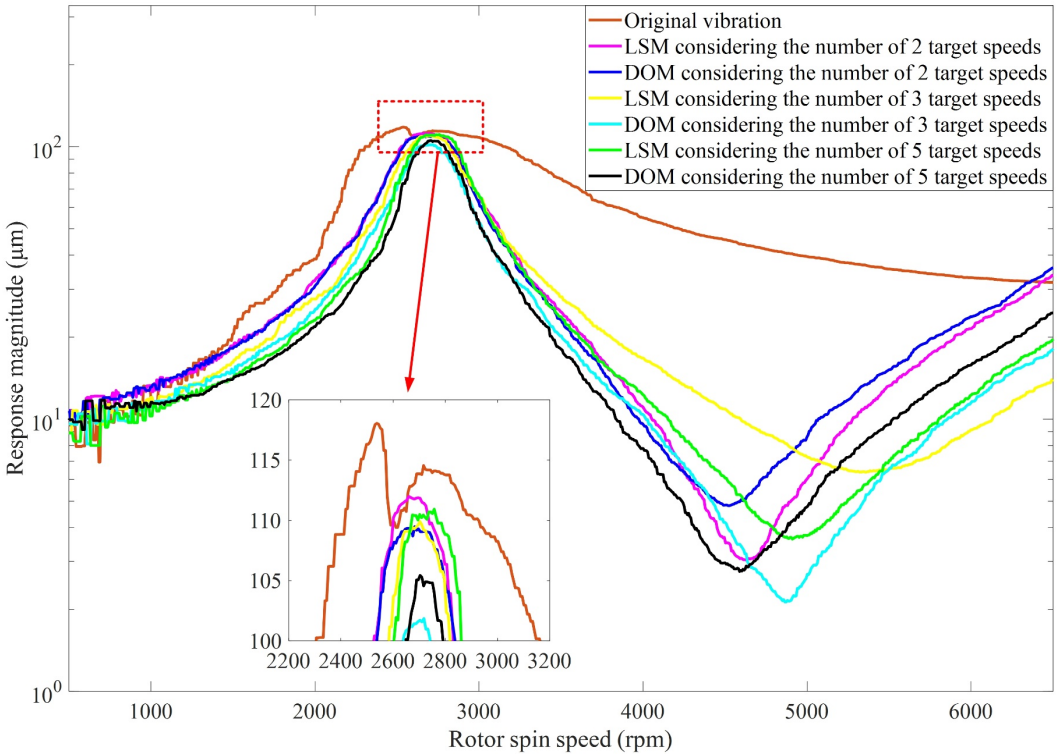

Fig.14 Speed-up curves at point #2 before and after balancing

Table 9. Results of the balancing for the different number of speed using LSM and DOM

Speed(rpm)	Measuring point	Original vibration	LSM		DOM	
		Amp (μm)	Amp (μm)	Percentage (%)	Amp (μm)	Percentage (%)
1500	1	41.94	35.89	14.4	35.71	14.9
	2	20.21	17.41	13.9	17.27	14.5
4000	1	46.95	16.65	64.5	16.05	65.8
	2	55.9	11.5	79.4	10.32	81.5
1500	1	41.94	35.49	15.4	34.84	16.9
	2	20.21	15.26	24.5	14.65	27.5
4000	1	46.95	10.9	76.8	6.81	85.5
	2	55.9	17.29	69.1	10.94	80.4
6000	1	27.32	10.84	60.3	8.981	67.1
	2	33.11	8.924	73	10.69	67.7
1000	1	33.67	31.56	6.3	31.86	5.3
	2	9.74	10.39	-6.7	11.15	-14.5
1500	1	41.94	34.49	17.8	34.25	18.3
	2	20.21	13.63	32.6	13.7	32.2
4000	1	46.95	9.31	80.2	4.723	89.9
	2	55.9	12.63	77.4	8.129	85.4
5000	1	32.65	6.252	80.9	2.342	92.8
	2	39.85	3.596	91	4.593	88.5
6000	1	27.32	11.12	59.3	8.281	69.7
	2	33.11	11.92	64	15.45	53.3

It is possible to observe that the maximum amplitude drops provided by the two methods gradually increases with the increase of the number of target speeds. Moreover, the DOM maximum amplitude drop is larger than the one provided by the LSM. However, the percentage of the amplitude drop is negative at 1000 rpm for five speeds (Table 9), and the amplitude of the second measuring point increases after balancing.

Table 10. Comparison of two methods considering the number of the target speed

The number of speeds	The sum of squares of original vibrations	Method	The sum of squares of residual vibrations	The maximum value of residual vibration (μm)
2	7496	LSM	2001	35.89
		DOM	1937	35.71
3	9339	LSM	2107	35.49
		DOM	1789	34.84
5	13222	LSM	3043	34.49
		DOM	2922	34.25

The DOM performs better than the LSM for the target speeds considered, both in terms of decrease of the sum of the squares of the residual vibrations (Table 10 and Fig.15) and the maximum of the residual vibration (Table 9-10). With three balancing target speeds the decrease percentage of the sum of the squares of the residual vibrations at the maximum is 77.4% with the LSM and 80.8% with the DOM (Fig.15). The experimental analysis shows that when the flexible rotor features a first critical speed within the operational speed range and a multiple speeds balance is adopted, three speeds can be taken into account at the same time to obtain an improved

balancing.

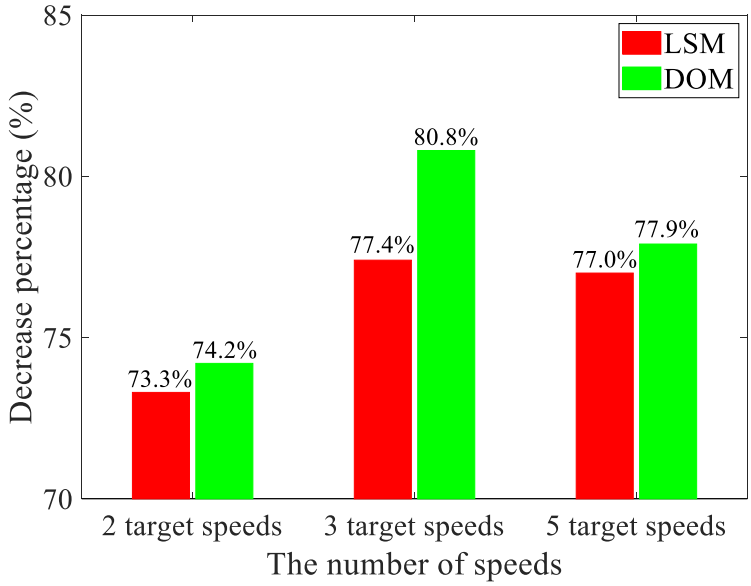

Fig.15 Comparison of the decrease percentage of the sum of the squares of the residual vibrations with LSM and DOM approach versus the number of target speeds

6 Conclusion

This paper has presented a balancing method for flexible rotor that involves a dual-objective optimization procedure. The method makes use of the global search and multi-points optimization characteristics of genetic algorithms when solving the first optimization objective function, so that the correction weight obtained represents the optimal solution from the current population. The second optimization scheme minimizes the maximum of the residual vibration, while ensures the identification of the minimum of the squared residual vibration. Simulation and experimental results show that the DOM provides a better balancing than the one calculated through the GA and the LSM when the rotor system a multi-speeds dynamic balancing. The number of speeds considered during the dynamic balancing has also a significant impact on the overall balancing effect. Experiments show that three speeds are needed to be considered simultaneously for an efficient dynamic balancing in a flexible rotor containing a first critical speed in the operational regime. The DOM here proposed is not only easy to operate but can also achieve both the minimum of the residual vibration of the rotor, and the maximum value of the same residual vibration. The proposed method can therefore be used for the practical balancing of flexible rotors in rotating machinery.

Funding

The research was supported by the National Natural Science Foundation of China (51975037).

References

[1] Y. Liu, Y.L. Zhao, J.T. Li, H. Ma, Q. Yang, X.X. Yan. Application of Weighted Contribution Rate of Nonlinear Outp ut Frequency Response Functions to Rotor Rub-impact, Mechanical Systems and Signal Processing, 136 (2020)106518.doi. 1 0.1016/j.ymssp.2019.106518.

[2] H.T. Shi, X.T. Bai, K. Zhang, Y.H. Wu, G.D. Yue, Influence of uneven loading condition on the sound radiation of st arved lubricated full ceramic ball bearings. Journal of Sound and Vibration, 461(2019)114910.doi:10.1016/j.jsv.2019.114910.

[3] R.E.D. Bishop, The vibrations of rotating shafts, J. Mech. Eng. Sci. 1 (1959) 55 [53].

[4] T.P. Goodman, A least-squares method for computing balance corrections, Transaction of the American Society of Mechanical

Engineers, Journal of Manufacturing Science and Engineering 86 (1964) 273-277.

[5] L.S. Qu, H. Qiu, G.H. Xu, Rotor balancing based on holospectrum analysis: principle and practice, China Mechanical Engineering 9 (1998) 60-63 (in Chinese).

[6] S. Liu, L.S.Qu, A new field balancing method of rotor systems based on holospectrum and genetic algorithm, Applied Soft Computing 8 (2008) 446-455, doi:10.1016/j.asoc.2006.11.012.

[7] S. Liu, A modified low-speed balancing method for flexible rotors based on holospectrum, Mechanical Systems and Signal Processing. 21 (2007) 348-364, doi:10.1016/j.ymssp.2005.09.009.

[8] X.X. Yu, K.M. Mao, S. Lei, Y.M. Zhu. A new adaptive proportional-integral control strategy for rotor active balancing systems during acceleration, Mechanism and Machine Theory. 136 (2019) 105–121, doi: 10.1016/j.mechmachtheory.2019.02.015.

[9] J.C. Fang, Y.G. Wang, B.C. Han, S.Q. Zheng. Field Balancing of Magnetically Levitated Rotors without Trial Weights, Sensors. 13(2013)16000-16022, doi: 10.3390/s131216000.

[10] Y. A. Khulief, M. A. Mohiuddin, M. El-Gebeily. A New Method for Field-Balancing of High-Speed Flexible Rotors without Trial Weights, International Journal of Rotating Machinery 2014(2014)1-11, doi: 10.1155/2014/603241.

[11] C. Liu, G. Liu, Field Dynamic Balancing for Rigid Rotor-AMB System in a Magnetically Suspended Flywheel, IEEE/ASME Transactions on Mechatronics 21(2016)1140-1150, doi: 10.1109/TMECH.2015.2495225

[12] A.M. Wang, X.H. Cheng, G.Y. Meng, Y. Xia, L. Wo, Z.Y. Wang, Dynamic analysis and numerical experiments for balancing of the continuous single-disc and single-span rotor-bearing system, Mechanical Systems and Signal Processing 86 (2017) 151-176, doi: 10.1016/j.ymssp.2016.09.034.

[13] G.F. Bin, X.J. Li, Y.P. Shen, W.W. Wang, Development of whole-machine high speed balance approach for turbomachinery shaft system with N+ 1 supports, Measurement 122(2018)368-379, doi: 10.1016/j.measurement.2018.02.035.

[14] D.-J. Han, Generalized modal balancing for non-isotropicrotor Systems, Mechanical Systems and Signal Processing21(2007) 2137-2160, doi: 10.1016/j.ymssp.2006.09.004.

[15] M.B. Deepthikumar, A.S. Sekhar, M.R. Srikanthan, Modal balancing of flexible rotors with bow and distributed unbalance, Journal of Sound and Vibration 332 (2013) 6216-6233, doi: 10.1016/j.jsv.2013.04.043.

[16] Y. A. Khulief, Wasiu. Oke, M. A. Mohiuddin, Modally Tuned Influence Coefficients for Low-Speed Balancing of Flexible Rotors, Journal of Vibration and Acoustics 136(2014) 024501-024505, doi: 10.1115/1.4025995.

[17] S. Tresser, A. Dolev, I. Bucher, Dynamic balancing of super-critical rotating structures using slow-speed data via parametric excitation, Journal of Sound and Vibration 415 (2018) 59-77, doi: 10.1016/j.jsv.2017.11.029.

[18] X.F. Li, L.X. Zheng, Z.X. Liu, Balancing of flexible rotors without trial weights based on finite element modal analysis, Journal of Vibration and Control 19(2013) 461-470, doi: 10.1177/1077546311433916.

[19] X.F. Wang, SQP algorithms in balancing rotating machinery, Mechanical Systems and Signal Processing 21 (2007) 1469–1478, doi: 10.1016/j.ymssp.2006.06.003.

[20] T. Messager, M. Pyrz, Discrete optimization of rigid rotor balancing, Journal of Mechanical Science and Technology 27(8)(2013) 2231-2236, doi: 10.1007/s12206-013-0605-x.

[21] M.V. Saldarriaga, V.S. Jr, J.D. Hagopian, J. Mahfoud, On the balancing of flexible rotating machines by using an inverse problem approach, Journal of Vibration and Control 17(2011) 1021-1033, doi: 10.1177/1077546310370669.

[22] Y. Kang, T.-W. Lin, Y.-J. Chang, Y.-P. Chang, C.-C. Wang, Optimal balancing of flexible rotors by minimizing the condition number of influence coefficients, Mechanism and Machine Theory 43 (2008) 891-908, doi: 10.1016/j.mechmachtheory.2007.06.005.

[23] C.D. Untaroiu, P.E. Allaire, W.C. Foiles, Balancing of Flexible Rotors Using Convex Optimization Techniques: Optimum Min-Max LMI Influence Coefficient Balancing, Journal of Vibration and Acoustics 130(2008) 021006-021010, doi: 10.1115/1.2730535.

[24] G.X. Li, Z.L. Lin, P.E. Allaire, Robust Optimal Balancing of High-Speed Machinery Using Convex Optimization, Journal of Vibration and Acoustics 130(2008) 031008-031018, doi: 10.1115/1.2890405.

[25] V.N. Carvalho, B.F.R. Rende, A. D.G. Silva, A.A. Cavalini, Jr., V. Steffen, Jr, Robust Balancing Approach for Rotating Machines Based on Fuzzy Logic, Journal of Vibration and Acoustics 140(2018) 051018-051026, doi: 10.1115/1.4039801.

[26] J.F. Yao, L. Liu, F.Y. Yang, F. Scarpa, J.J, Gao, Identification and optimization of unbalance parameters in rotor-bearing systems, Journal of Sound and Vibration 431(2018) 54-69. doi.org/10.1016/j.jsv.2018.05.050.

[27] Z. Wang, Rotor dynamics design of rotating machinery, Tsinghua University Press, Beijing, 2015, pp. 48-49. (in Chinese).

[28] Z.H. Jia, H.P. Chen, Y.H. SUN, Multi-objective Particle Swarm Optimization Algorithm for Flexible Job Scheduling, Journal of Chinese Computer Systems 29 (2008) 885-889 (in Chinese).

[29] J.H. Holland, Adaptation in Natural and Artificial Systems, second ed., Cambridge, Massachusetts, London, England, The MIT press, 1992.

[30] I.G. Tsoulos, I.E. Lagaris, GenMin: An enhanced genetic algorithm for global optimization, Computer Physics Communications 178 (2008) 843-851, doi:10.1016/j.cpc.2008.01.040.

[31] A.R. Ayad, H.A. Awad, A.A. Yassin, Parametric analysis for genetic algorithms handling parameters, Alexandria Engineering Journal 52 (2013), 99-111, doi: 10.1016/j.aej.2012.10.007.

[32] A. Robison, A. Vacca, Multi-objective optimization of circular-toothed gerotors for kinematics and wear by genetic algorithm, Mechanism and Machine Theory 128 (2018) 150–168, doi: 10.1016/j.mechmachtheory.2018.05.011.

[33] T.C. Pak, Y.C. Ri, Optimum designing of the vapor compression heat pump using system using genetic algorithm, Applied Thermal Engineering 147 (2019) 492–500, doi: 10.1016/j.applthermaleng.2018.07.063.